Hydrogen passivation of interstitial iron in boron-doped multicrystalline silicon during annealing

AnYao Liu, Chang Sun, and Daniel Macdonald

Citation: Journal of Applied Physics **116**, 194902 (2014); doi: 10.1063/1.4901831
View online: http://dx.doi.org/10.1063/1.4901831
View Table of Contents: http://scitation.aip.org/content/aip/journal/jap/116/19?ver=pdfcov
Published by the AIP Publishing

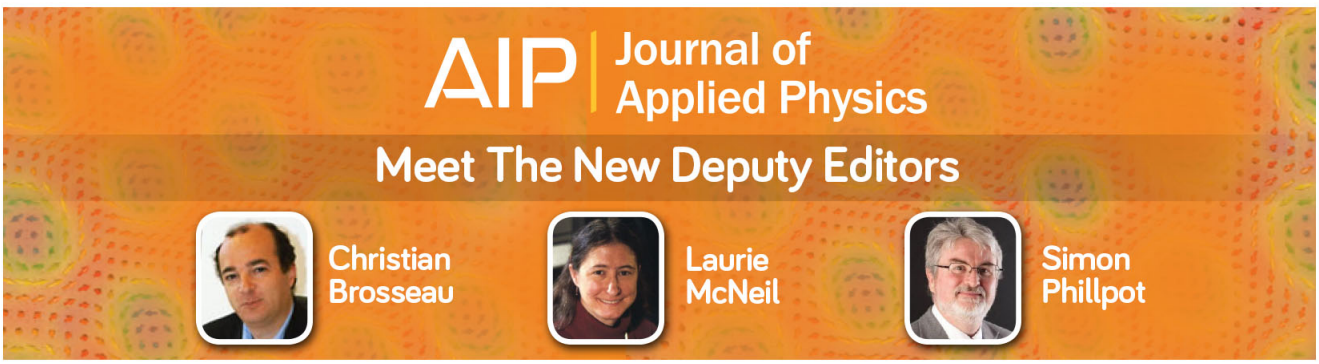

Hydrogen passivation of interstitial iron in boron-doped multicrystalline silicon during annealing

AnYao Liu, Chang Sun, and Daniel Macdonald
Research School of Engineering, the Australian National University, Canberra, ACT 0200, Australia

(Received 11 August 2014; accepted 4 November 2014; published online 21 November 2014)

Effective hydrogenation of interstitial iron in boron-doped multicrystalline silicon wafers is reported. The multicrystalline silicon wafers were annealed with plasma-enhanced chemical vapour deposited silicon nitride films, at temperatures of 400 °C – 900 °C and for times from minutes to hours. At low temperatures where a combined effect of hydrogenation and precipitation of dissolved Fe is expected, results show that the hydrogenation process dominates the effect of precipitation. The concentrations of dissolved interstitial iron reduce by more than 90% after a 30-min anneal at temperatures between 600 and 900 °C. The most effective reduction occurs at 700 °C, where 99% of the initial dissolved iron is hydrogenated after 30 min. The results show that the observed reductions in interstitial Fe concentrations are not caused by the internal gettering of Fe at structural defects or by an enhanced diffusivity of Fe due to the presence of hydrogen. The hydrogenation process is conjectured to be the pairing of positively charged iron with negatively charged hydrogen, forming less recombination active Fe-H complexes in silicon. © *2014 AIP Publishing LLC*.
[http://dx.doi.org/10.1063/1.4901831]

I. INTRODUCTION

Iron (Fe) is a common contaminant in silicon, especially prevalent in multicrystalline silicon (mc-Si) materials.[1–3] Iron significantly degrades the silicon material quality by acting as deep-level recombination centres, leading to reduced minority carrier lifetime and solar cell efficiency.[1,4] Mitigating the detrimental effect of Fe in silicon is therefore of great interest. External gettering of Fe during a phosphorous diffusion step at high temperatures is the most common and effective method used in the photovoltaic industry.[5] The efficacy of this external gettering process can be further improved by a follow-up anneal at lower temperatures for extended hours, taking advantage of the increased segregation ratio between the gettering layer and the wafer bulk.[6–8] The process of external gettering moves the dissolved Fe atoms from the silicon bulk to the diffused regions on the wafer surfaces, achieving a reduction of the dissolved Fe concentration in the bulk by 1–2 orders of magnitude or more.[5,9] Internal gettering of Fe by the structural defects in mc-Si has also been shown to cause a reduction of the dissolved Fe concentration by 1–2 orders of magnitude.[10] This process, however, is generally slower, as it requires low to moderate temperatures to reduce the Fe solubility limit enough to drive precipitation, and the Fe diffusivity at such temperatures becomes one of the limiting factors.[10] To achieve very thorough removal of the dissolved iron atoms, both external and internal gettering processes require long hours.

The benefit of hydrogen for silicon materials has been widely recognised. Hydrogen is known to passivate a wide range of defects and impurities in silicon, including vacancies, extended defects, shallow dopants, non-metallic and metallic impurities.[11,12] Several authors reported a reduction of the electrical activity and concentration of iron point defects after the incorporation of atomic hydrogen into the silicon bulk.[13–18] Studies using deep-level transient spectroscopy (DLTS) shows that the peaks of iron-related energy levels disappear or reduce after either hydrogen plasma exposure[14] or hydrogen ion implantation.[13] The concentrations of dissolved interstitial iron are found to decrease after hydrogen incorporation, either via firing of hydrogen-containing silicon nitride films[15–17] or exposure to a hydrogen plasma.[18] The exact mechanism for this phenomenon, however, remains unclear. While some attribute it to the hydrogen passivation of iron,[13–17] others believe it to be the gettering of metals by hydrogen-enhanced metal diffusivity.[18,19] In either case, the presence of hydrogen provides an additional method for reducing the harmful impact of dissolved Fe in silicon. In addition, the process has the potential to be more time efficient than the external or internal gettering processes, due to the high diffusivity of hydrogen in silicon.[20]

In this paper, we aim to study the mechanism for the reduced interstitial iron concentration after hydrogen incorporation into multicrystalline silicon. Atomic hydrogen is introduced into the mc-Si bulk via annealing the wafers with plasma-enhanced chemical vapour deposited (PECVD) silicon nitride (SiN_x) films, which is a common solar cell fabrication step for the firing of metal contacts. In this study, annealing was carried out for a range of temperatures from 400 °C to 900 °C and for times from 3 min to 5 h. To distinguish the effect of hydrogen from coincident temperature-driven effects, such as precipitation at structural defects, sister mc-Si wafers are subject to the same annealing steps in the absence of atomic hydrogen. A recent study by Hallam *et al.*[21] has shown that the possible hydrogenation of boron-oxygen defects depends on the presence of light-generated excess carriers, which is thought to change the charge states of hydrogen. In this paper, we also study the effect of illumination on the hydrogenation of iron through simulation and experiments. The minority carrier lifetime and the

concentration of interstitial Fe atoms are measured by the calibrated photoluminescence (PL) imaging technique.[22–24] This also enables the examination of the changes in the spatial distributions on high resolution lifetime and Fe images before and after different anneals, providing further insights into the hydrogenation mechanism.

II. EXPERIMENT

The multicrystalline silicon wafers were sourced from a commercially grown boron-doped directionally solidified ingot. Sister wafers located at 29% from the bottom of the ingot were chosen for this study, with a resistivity of around 1.4 Ω cm. The $12.5 \times 12.5\,cm^2$ wafers were diced into smaller pieces of $4.15 \times 4.15\,cm^2$ in size for ease of processing. The mc-Si wafers have an average grain size of $17\,mm^2$ with a standard deviation of $50\,mm^2$, as a result of a large variation in grain sizes. The samples were then chemically polished, resulting in final thicknesses in the range of 280–300 μm. Float-zone (FZ) boron-doped silicon wafers of 1.7 Ω cm and 240 μm thickness were also included and were subjected to the same processing steps, in order to monitor surface passivation and possible process contamination.

Some of the wafers were cleaned and passivated by silicon nitride (SiN_x) films using PECVD. Although the set temperature for the PECVD reactor is 450 °C, the actual temperature on the samples during the deposition process, as measured by an infrared sensor, is about 250 °C. The deposited SiN_x films are 80 nm thick. Some of the samples were then annealed at 400 °C in a quartz tube furnace in a nitrogen ambient for various cumulative times. Some degradation of the SiN_x films was observed after the 400 °C anneals on the FZ samples. However, the minority carrier lifetime due to surface recombination remained much higher than the lifetime of the mc-Si wafers, which are limited by the bulk defects. Hence, surface degradation does not affect the measured effective lifetime and interstitial Fe concentrations. Re-coating of the SiN_x films was therefore not required for the samples annealed at 400 °C. Some of the other SiN_x coated samples were annealed in a rapid thermal processor (RTP), whose heating functionality comes from pulsing infrared lamps. This represents the case of annealing under illumination.

Further samples were prepared for studies at higher annealing temperatures of 600–900 °C. To distinguish the influence of hydrogen from temperature-induced effects, two sets of wafers underwent the same thermal annealing steps—one with the hydrogen source present via SiN_x films, and the other without hydrogen, with thermally grown silicon oxide (SiO_2) layers providing surface passivation. The two sets are pairs of sister wafers. To ensure the same thermal history, both sets of the wafers were cleaned and annealed in dry oxygen at 1000 °C for 1 h, followed by an anneal in nitrogen for 30 min, before being cooled down to 750 °C at 10 °C/min and then left in a high air flow to cool to room temperature within minutes. This results in the growth of SiO_2 layers as surface passivation. The high temperature process also homogenises the distributions of interstitial Fe across the mc-Si wafers. One set of the wafers were then dipped in dilute HF solution to remove the SiO_2 layers and were re-passivated using PECVD SiN_x films. Each pair of the SiO_2 and SiN_x passivated samples was annealed for the same temperature and time. Short anneals of minutes were performed in an RTP (at these higher temperatures, the presence or not of illumination during annealing is not expected to have any impact, as described below), while long anneals were conducted in a quartz tube furnace. The SiN_x passivated samples were annealed in nitrogen, while the SiO_2 samples were annealed in forming gas in order to maintain the surface passivation effect. The forming gas used in this study consists of 95% argon and 5% hydrogen molecules. The presence of hydrogen, however, has little bulk hydrogenation effect, as the hydrogen is trapped by the defective Si-SiO_2 layers, which act as diffusion barriers for H_2 into the bulk.[25–27] This is confirmed by the results shown in this study, where little change in carrier lifetime and recombination activity of defects is found after annealing SiO_2 passivated mc-Si samples in the forming gas. The SiN_x coated samples experienced severe surface degradation after annealing at temperatures of 600–900 °C. Therefore, after each annealing step, the degraded SiN_x films were stripped off in dilute HF solution, and the samples were cleaned and re-passivated with fresh SiN_x films, in order to measure the bulk lifetime and Fe concentrations.

The minority carrier lifetime, interstitial Fe concentration ($[Fe_i]$) and resistivity were measured after each processing step. Resistivity was determined from dark conductance data measured using a quasi-steady-state photoconductance (QSSPC) tester[28] from Sinton Instruments. Spatial distributions of lifetimes and Fe_i concentrations were obtained by using a PL imaging system[22] from BT imaging. The carrier lifetimes from PL images were calculated by calibrating via an in-built QSSPC tester, using the method described in Ref. 23 to account for the inhomogeneity in mc-Si wafers. Calculation of the Fe_i concentration is based on the well-established method of monitoring the changes in minority carrier lifetimes before and after the dissociation of the Fe-B pairs via strong illumination.[24,29,30] The pixel size of the PL images is about 23 μm, although the actual resolution is largely limited by the carrier diffusion length. Most of the samples have low carrier lifetimes of a few microseconds, and thus the effect of carrier diffusion smearing on the resulting $[Fe_i]$ images is small.[31] A point spread function was applied to de-convolute image smearing caused by the lateral photon scattering within the Si-CCD camera.[32]

III. RESULTS

A. Hydrogen passivation of iron

1. Hydrogenation of iron during PECVD deposition

Fig. 1 shows a comparison of the average interstitial Fe concentrations of the same wafers in two states—after oxidation at 1000 °C, and after stripping off the SiO_2 layers followed by surface passivation using PECVD SiN_x. All of the tested wafers show reductions in the Fe_i concentrations, ranging from 10% to 30% after the PECVD surface passivation. The two different passivation methods result in different surface recombination lifetimes. However, the surface

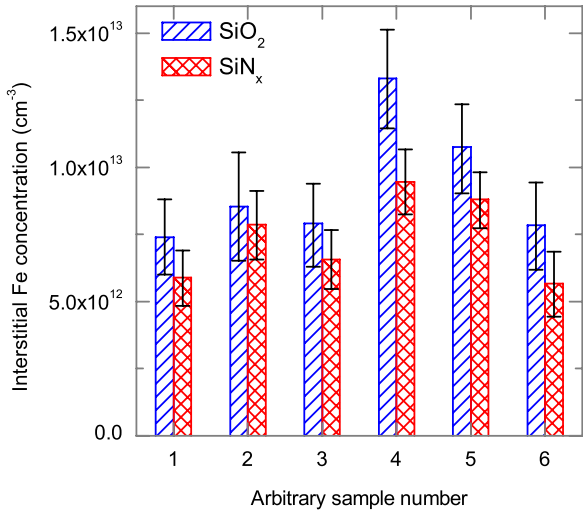

FIG. 1. Average interstitial Fe concentrations of the same wafers before (blue) and after (red) the PECVD SiN_x deposition.

recombination lifetime of either of the methods is still orders of magnitude higher than the lifetime due to bulk defects, resulting in similar measured effective carrier lifetimes of the mc-Si samples. In any case, the effect of surface passivation is cancelled out in the $[Fe_i]$ calculation. The differences in the Fe_i concentrations before and after PECVD are therefore not caused by the different passivation films, but reflect a real physical phenomenon. This was also observed previously[5] for FZ-Si wafers of known implanted Fe concentrations, which show slight reductions of $[Fe_i]$ after repetitive PECVD SiN_x depositions. Herzog *et al.*[33] reported improved bulk lifetime after the PECVD SiN_x depositions. The reduced interstitial Fe concentrations after PECVD as shown in Fig. 1 are therefore likely due to the hydrogenation of interstitial Fe during the PECVD processes.

The temperature of the samples during the PECVD depositions was monitored by an infrared sensor. In this experiment, the maximum temperature on the wafers during PECVD is about 250 °C, and the samples were kept at this temperature for only a few minutes for the deposition process, after which the samples were cooled down to 150 °C in half an hour before being removed from the reactor chamber. In comparison with the results of the 400 °C anneals in the latter part of this paper, and also those in literature,[18,34] this reduction in $[Fe_i]$ seems large for this deposition temperature and time. However, the deposition process consists of various complex reactions, including the presence of a plasma containing hydrogen and hence is not directly comparable to the process of annealing SiN_x films.

2. Effect of illumination

The fractions of the different charge states of interstitial iron (Fe^+ and Fe^o) and hydrogen (H^+, H^-, and H^o) under steady state can be estimated from their energy levels and capture cross sections, by using Shockley-Read-Hall (SRH) statistics.[35,36] Details of the model as applied to the case of hydrogen passivation in silicon can be found in Ref. 37 and in the upcoming publication by Sun *et al.*[38]

The hydrogenation of Fe may be due to the reaction of positively charged Fe and negatively charged H, forming stable and less recombination active Fe-H complexes. Other processes are also possible, such as the interaction between neutrally charged Fe and H. In this study, we consider the conjecture of positive Fe and negative H. The percentage of Fe^+ out of the total isolated interstitial Fe, and the percentage of H^- out of the total monatomic H, are simulated and shown in Fig. 2, as a function of temperature and excess carrier injection. The calculation considers the effect of band gap narrowing with temperature,[39] and assumes constant capture cross sections and constant distances between defect energy levels and the valence band, due to a lack of temperature-dependent data in the literature. As shown in Fig. 2, for a moderate injection level below $10^{16}\,cm^{-3}$, the effect of illumination on the percentages of charged species becomes negligible for temperatures higher than 400 °C, as the intrinsic carrier concentration becomes much higher than the excess carrier concentration. Hence, this is also true for the percentages of H^o and H^+.

Fig. 2 also shows that at temperatures above 400 °C, the fractions of both species increase with temperature. Note that the exact magnitude of the simulated fractions becomes increasingly inaccurate at higher temperatures, due to limited

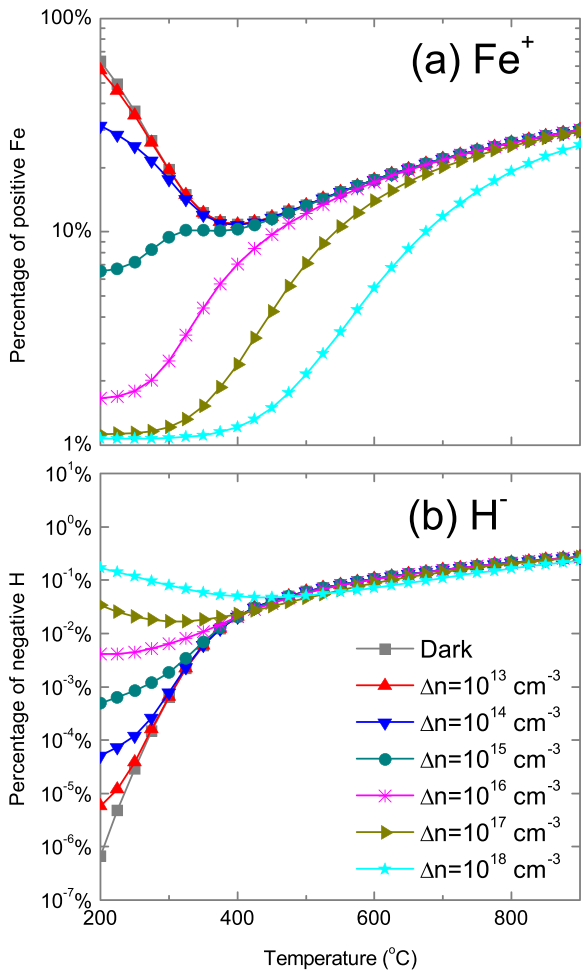

FIG. 2. Estimation of the percentage of the total isolated interstitial Fe concentration present in the positive charge state (Fe^+) (top); percentage of hydrogen present in the negative charge state (H^-) (bottom).

data in the literature on the temperature-dependent parameters. However, the increasing trends of the fractions are as expected from the increasingly symmetrical carrier distributions across the band gap as the temperature increases. As the fractions of Fe^+ and H^- increase with temperature, i.e., increasing concentrations of both reactants are available, and given that the reaction rate constant also increases with temperature as described by Arrhenius' equation, the reaction rate of Fe^+ and H^- pairing should also increase from 400 to 900 °C. It should be noted however that the reverse reaction (dehydrogenation) will, for the same reason, proceed with an increasing rate as the temperature increases, and at some point may come to dominate the forward reaction, leading to a net dehydrogenation effect.

To test the possible impact of illumination on the experiments presented here, SiN_x coated wafers were annealed at 400 °C for cumulative time durations, one in an RTP which provides illumination during annealing, and one in a dark quartz tube furnace. Degradation of the SiN_x films is more severe under strong flashing of the RTP, which was also observed in Ref. 17. The carrier lifetime due to surface recombination, as measured on the high quality FZ-Si samples, dropped from 1.7 ms to 80 μs after 50 min cumulative annealing in the RTP; while the surface lifetime for furnace annealed samples dropped to 110 μs after 5.5 h. Note that the surface lifetime is still at least one order of magnitude higher than the effective lifetime of the mc-Si samples, and thus the sensitivity of the [Fe_i] measurement was maintained. As a result of the different degradation rate, the RTP annealed sample could not reach a cumulative annealing time as long as the furnace annealed sample. As shown in Fig. 3, both of the mc-Si wafers experienced reductions in the interstitial Fe concentrations after annealing, and the concentrations follow an exponential decay curve. The exponential reduction time constants of the two wafers are found to be similar—170 min for the illuminated sample and 200 min for the sample annealed in the dark. The main mechanism that drives the reductions in Fe_i concentrations during the 400 °C anneals is therefore not affected by this illumination, confirming the charge state simulations shown above. Unfortunately, precise illumination intensities during RTP are not known, but it is likely that the carrier injection levels remain below 10^{16} cm^{-3}.

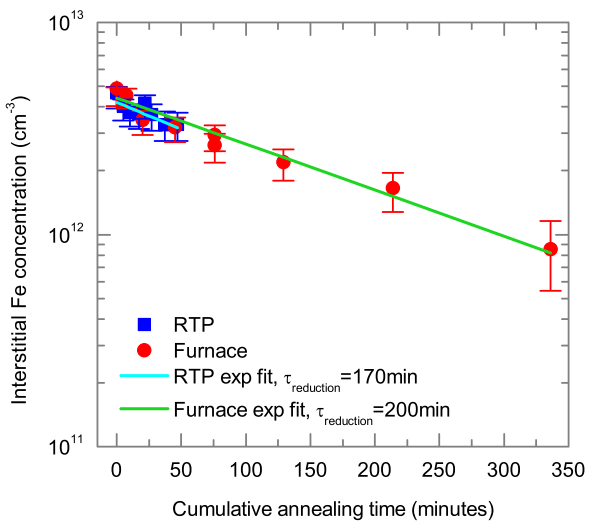

FIG. 3. Interstitial Fe concentration with respect to the cumulative annealing time for two wafers annealed at 400 °C with SiN_x films, one annealed under illumination (RTP), and one in the dark (quartz tube furnace).

The presence of atomic hydrogen is identified as the crucial element for the observed [Fe_i] reductions. In our previous work,[10] mc-Si wafers from the same part of this ingot were also annealed at 400 °C in dark, one with SiO_2 (i.e., no hydrogen source) and one with Al_2O_3 (i.e., with hydrogen source) passivation layers. The SiO_2 passivated wafer resulted in a [Fe_i] reduction time constant of 1200 min, while the one with Al_2O_3 films gave a time constant of 210 min. In Ref. 34, a SiN_x coated mc-Si wafer annealed at 400 °C shows a [Fe_i] reduction time constant of 100 min. In Ref. 18, atomic hydrogen was introduced into the silicon bulk by subjecting mc-Si wafers to a hydrogen plasma at 400 °C. From the changes in [Fe_i] after the hydrogen plasma step, the average reduction time constant is estimated to be 280 ± 85 min. All of the reported [Fe_i] reduction time constants for mc-Si wafers annealed at 400 °C with the presence of atomic hydrogen sources, either from Al_2O_3 films,[10] SiN_x films,[34] or hydrogen plasma,[18] are comparable with our findings here (Fig. 3). This confirms the effect of hydrogen on the observed [Fe_i]. Since the reduction time constants of 170 min and 200 min for the SiN_x annealed samples are much smaller than the 1200 min measured on wafers with no hydrogen source, the trends presented in Fig. 3 are therefore dominated by the hydrogen effect.

3. Effect of temperature

Fig. 4 presents the average interstitial Fe concentrations of wafers before and after different annealing steps, for a range of temperatures from 400 °C to 900 °C, and for two sets of samples—one with SiO_2 and one with SiN_x passivation layers, that is, without and with the hydrogen source during annealing. Different changes in the Fe_i concentrations can be observed between the two sets. For the SiO_2 samples, after annealing at 400–700 °C, some reductions in the Fe_i concentrations are observed, due to Fe precipitation;[10] while at 800–900 °C, the [Fe_i] of the SiO_2 set remains almost unchanged within the error bars after anneals of 3 min and 30 min, and an increase in [Fe_i] is seen after annealing at 900 °C for 5 h, as a result of the dissolution of Fe precipitates.[40] This behaviour is consistent with the solubility-limit driven precipitation and dissolution of Fe which has been observed before and in our own recent study on the same material.[10] That is, the changes in [Fe_i] of the SiO_2 samples demonstrate the effect of temperature. On the other hand, the SiN_x coated wafers, which were subjected to the same thermal anneals, consistently show much greater reductions in the Fe_i concentrations, for the entire temperature range of 400–900 °C.

The Fe images of the SiN_x coated wafers annealed at various temperatures all show that the reductions of [Fe_i] occur homogeneously across the wafer. An example can be seen in Figs. 5(k)–5(n) for a sample annealed at 700 °C. Note that the PL and Fe images of the SiN_x sample after 30 min

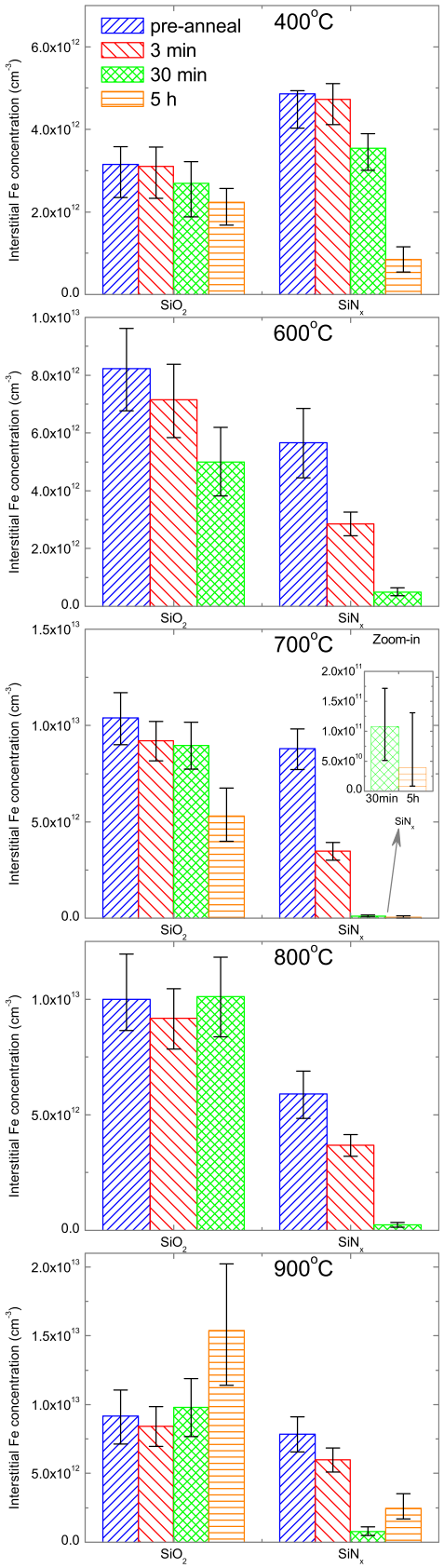

FIG. 4. Interstitial Fe concentrations across wafers with SiO_2 passivation (no hydrogen source) and wafers with SiN_x films (with hydrogen source) in the pre-annealed state, after annealing for short time (3 min for those at 400–800 °C and 140 s at 900 °C), after annealing for 30 min, and after 5 h (only for the 400 °C, 700 °C, and 900 °C anneals). Note that the comparisons of the SiO_2 and SiN_x passivated wafers are made on sister wafers, except for the pair annealed at 400 °C.

annealing are more smeared out than the rest, because of a large increase in the carrier diffusion length. The homogeneous [Fe_i] reduction is different from the effect of Fe precipitation, either during ingot cooling[31] or during annealing,[10] where the denuded zones of reduced [Fe_i] near grain boundaries can be clearly seen on the Fe images.[10,31] The SiO_2 sister wafers show the appearance of such denuded zones near some of the grain boundaries after annealing (although not so clear on logarithmically scaled Fe images). This is an additional proof that the greater reductions in [Fe_i] of the SiN_x coated wafers are not caused by the accelerated gettering of Fe by the grain boundaries due to hydrogen-enhanced Fe diffusivity. Furthermore, at high temperatures of 800 °C and 900 °C, the respective Fe solubility limits[4] are comparable or higher than the concentrations of Fe_i in the wafers, and thus Fe precipitation should not occur. Therefore, by comparing the changes in [Fe_i] of the SiO_2 and SiN_x sister wafers and examining the spatial changes in [Fe_i] across the mc-Si wafers, it is clear that the observed decreases in [Fe_i] of the SiN_x set are not due to accelerated Fe precipitation, but some other impact of the presence of hydrogen.

Hydrogenation of shallow dopants in silicon, such as boron, is well known.[11,12] However, the passivated boron should be reactivated by annealing at temperatures higher than 160 °C,[11] which is lower than the PECVD process temperature. In addition, the boron concentration of the tested samples is $10^{16}\,cm^{-3}$, which is 3–4 orders of magnitude higher than the dissolved Fe concentration, meaning that a moderate change in the [B] is unlikely to affect the measurement of [Fe_i]. To confirm that the observed changes in interstitial Fe concentrations are not due to changes in the boron concentration, the resistivities of both SiO_2 and SiN_x samples in the as-cut state, and before and after different annealing steps, were monitored by QSSPC dark conductance measurements. The resistivities were found to stay the same throughout the annealing steps and also between the SiO_2 and SiN_x sister wafers. The measured reductions in [Fe_i] of the SiN_x coated samples are therefore not due to the hydrogenation of boron.

With increasing annealing time from 3 min to 30 min, all of the samples annealed at 400–900 °C show further reductions of the Fe_i concentrations, as can be seen in Figs. 4 and 6. After 30 min, reductions of more than 90% of the original Fe_i concentrations have been achieved for samples annealed at 600–900 °C, that is, those which require recoating of SiN_x films in between the anneals. The impact of hydrogenation during the PECVD process, as disucssed above, is thus small compared to the effect of annealing. Some of the wafers, which were annealed at 400 °C, 700 °C, and 900 °C, were subjected to further anneals of 5 h. As shown in Figs. 4 and 6, the 5 h anneals result in further reductions in Fe_i concentrations for those at low temperatures of 400 °C and 700 °C; whereas, for the 900 °C, this additional 5 h anneal leads to an increase in the [Fe_i] compared to the previous 30 min anneal. However, the SiO_2 sister wafer also shows an increase in the Fe_i concentration after the same annealing step. Therefore, the observed increase in [Fe_i] of the SiN_x sample could be related to the effect of precipitate dissolution which offsets the hydrogenation of dissolved Fe. Alternatively, this increase could also

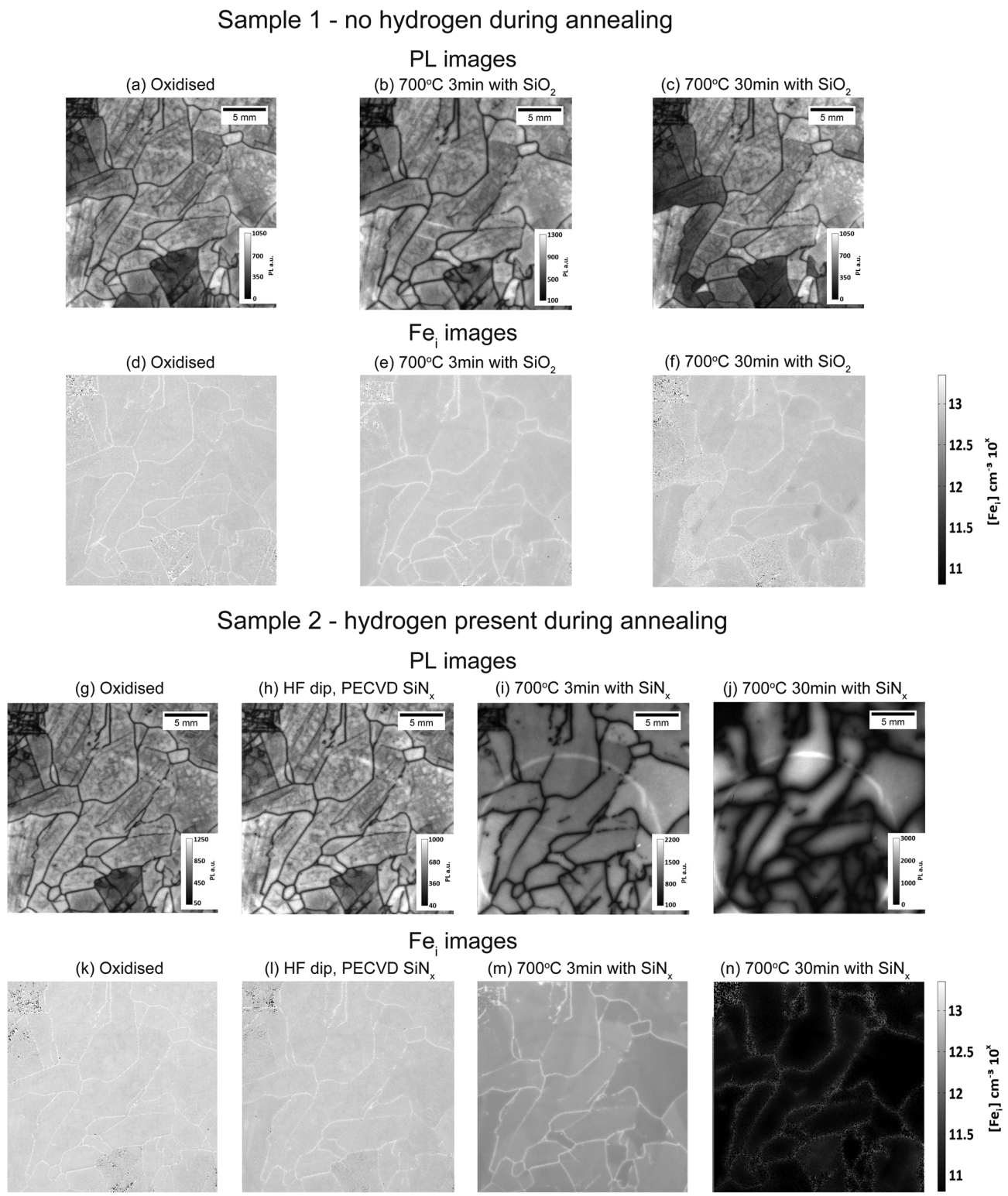

FIG. 5. Photoluminescence images [sub-figures (a)–(c) and (g)–(j)] and the corresponding interstitial Fe concentration images [(d)–(f) and (k)–(n)] of a pair of sister wafers which underwent the same anneals at 700 °C, with [(g)–(n)] and without [(a)–(f)] hydrogen source during annealing. Note that while the scales of the PL images (PL counts of arbitrary unit) vary to demonstrate the grain features, the Fe images have the same logarithmic scale to compare the concentrations and distributions of Fe_i. The large "rings" appearing on the PL images are the QSSPC coil in the PL imager.

be caused by the increasing dominance of the dehydrogenation of Fe as time increases. It was found in Ref. 41 that increased annealing times actually cause degradation of carrier lifetime for edge-defined film-fed (EFG) and string ribbon silicon, and the effect was attributed to dehydrogenation. It is known that during annealing the flux of hydrogen from the SiN_x film into the silicon bulk slows down as time increases and the diffusivity of H is rather high.[20] Hence, the reaction of H binding with defects and impurities in mc-Si would dominate at the beginning of the anneals. However, as

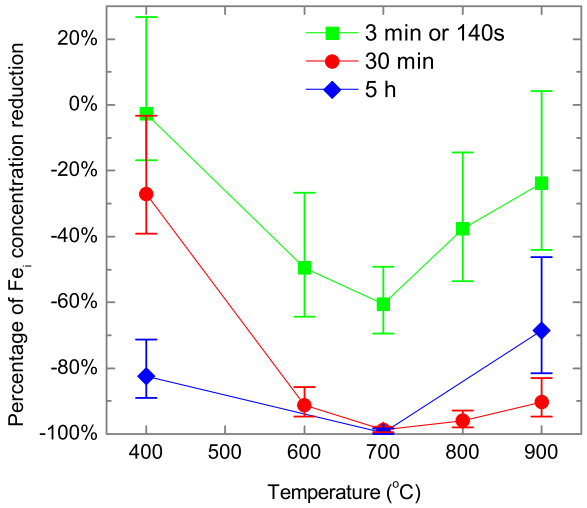

FIG. 6. Percentage of the [Fe_i] reduction after annealing with respect to the pre-annealed states, for wafers with SiN_x coatings. The plot includes results of annealing at 400–900 °C and for different cumulative times (although re-coating was performed after each annealing step). Lines are guides to the eyes.

the annealing time increases, without constant replenishment of the H concentration from the films, the effusion of H out of the sample will start to dominate, the hydrogenation reaction will slow down, at some point allowing the reverse reaction of H-defect dissociation (i.e., dehydrogenation) to begin to dominate.

Fig. 6 plots the percentage reductions of the Fe_i concentrations after annealing with the SiN_x samples, compared to the respective pre-annealed states, for different annealing temperatures and times. As shown in Fig. 6, for the same annealing times of 3 min, 30 min, and 300 min, the most effective reduction of the Fe point defect occurs at 700 °C. Note that the 900 °C short anneal was 140 s instead of 3 min, because of equipment limitations. Hydrogen diffuses rapidly in silicon,[12,20] and therefore the hydrogenation process is generally not diffusion-limited,[17] especially at such high temperatures. For all of the tested annealing time durations, the [Fe_i] reduction effectiveness increases with temperature from 400 to 700 °C. This agrees with the simulations shown in Fig. 2, which indicate that the Fe^+ and H^- pairing rate should increase with temperature above 400 °C. Then from 700 to 900 °C, the reduction of [Fe_i] becomes less effective. This may be attributed to either the dissolution of Fe precipitates or the reverse reaction of Fe-H dissociation, that is, dehydrogenation, or a combination of both. Note that the effect of Fe precipitate dissolution is negligible for short annealing times of 3 min and 30 min, as reflected by the small changes in the [Fe_i] of the SiO_2 sister wafers shown in Fig. 4. Dehydrogenation is therefore the more likely explanation, as the measured Fe_i concentrations are the net effects of hydrogenation and dehydrogenation of Fe_i. The effectiveness of hydrogenating defects in EFG and string ribbon silicon was also found to decrease at temperatures higher than 750 °C, as a result of dehydrogenation.[41]

B. Hydrogen passivation of other defects

A high density of intra-grain defects were activated after the initial oxidation step at 1000 °C. This is clear when

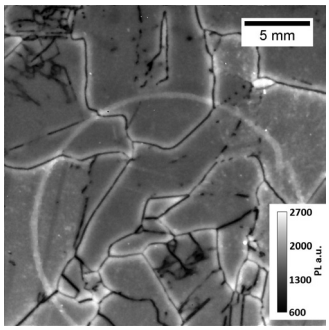

FIG. 7. PL image of a neighbouring wafer to the two samples shown in Fig. 5. The wafer was chemically polished and passivated using PECVD SiN_x, to show the grain structures of mc-Si in the as-cut state. Note that the "ring" is the QSSPC coil.

comparing the PL images of the oxidised samples in Figs. 5(a) and 5(g) with a neighbouring wafer in the as-cut state in Fig. 7. The as-cut neighbouring wafer was simply chemically polished and then passivated with PECVD silicon nitride, without any further steps, to allow examination of the bulk features in the as-cut state. As shown in Figs. 5(g) and 5(h), these activated defects remain unchanged after the PECVD SiN_x deposition but were fully deactivated after a short hydrogenation step of 3 min (Fig. 5(i)), and they remain passivated during the subsequent long time anneals. On the other hand, wafers without the high temperature step show no such drastic change in the recombination activity of structural defects after hydrogenation. An example is shown in Fig. 8, which shows the PL images of a sample before and after hydrogenation, and the sample did not undergo any high temperature process prior to hydrogenation. As can be seen by comparing Fig. 8 with Figs. 5(h)–5(i), the intra-grain defects already present in the as-cut state are less readily hydrogenated than the defects activated after a high temperature process. This agrees with the observations reported in Ref. 42.

The structural defects in mc-Si, for example, dislocations and grain boundaries, become recombination active after being decorated by impurities.[43] By comparing the PL images with the corresponding Fe images in Fig. 5, it can be seen that these high temperature activated defects are not related to interstitial Fe. Buonassisi *et al.*[40] reported that after rapid thermal annealing at 860 °C and 1000 °C, copper and nickel silicide precipitates are almost entirely dissolved.

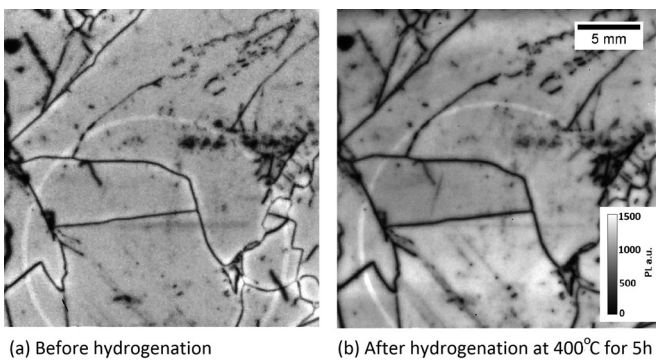

FIG. 8. PL images of the same wafer (a) in the as-cut state, that is, the wafer was only chemically polished and passivated using PECVD SiN_x and (b) after hydrogenation at 400 °C for 5 h.

Recombination activity of the intra-grain regions was also found to increase,[40] and the spatial distributions look similar to the PL images from this study. Therefore, the activated defects may be due to the decoration of intra-grain dislocations by dissolved impurities, such as copper and nickel, and are then effectively hydrogenated during the subsequent anneals.

From the measured effective minority carrier lifetime (τ_{eff}) and the concentration of interstitial Fe ([Fe_i]), the carrier lifetime due to recombination channels other than Fe_i, τ_{other}, can be estimated. The changes in τ_{eff}, τ_{other}, and [Fe_i] before and after annealing for different times are shown in Fig. 9, for the samples annealed at 400 °C, 700 °C, and 900 °C. The changes in τ_{eff} and τ_{other} are small for the SiO_2 sample set, indicating that the observed large changes in lifetimes for the SiN_x set are due to hydrogen. As shown in Fig. 9, with increasing annealing time, the Fe_i concentrations decrease and the effective carrier lifetimes increase. The only exception is after the 900 °C 5 h anneal, which resulted in a decrease in effective lifetime and an increase in [Fe_i], possibly because of the dissolution of impurities including Fe precipitates, or dehydrogenation, as discussed above.

On the other hand, τ_{other} first increases and then decreases to lower than the pre-annealed τ_{other} values with annealing time. The trend of τ_{other} with time could be related to the shifting dominance from hydrogenation to dehydrogenation as annealing proceeds, as a result of the effusion of hydrogen from the sample. This has less of an impact on interstitial Fe, as shown by the different time at which maximum τ_{other} and minimum [Fe_i] occur (Fig. 9). The concentration of H from PECVD SiN_x films is orders of magnitude higher than the concentration of interstitial Fe in mc-Si,[20] and therefore Fe_i is less susceptible to the loss of hydrogen. The different response of interstitial Fe and other defects to the hydrogenation time could also be due to the different hydrogenation activation and deactivation energies for different species, leading to different sensitivity to the concentration changes in the reacting species. The optimum hydrogenation time for other defects is 45 min at 400 °C and is 3 min at 600–900 °C. However, note that at 600–900 °C, very coarse time intervals were examined. The longer optimum hydrogenation time at a lower temperature can be explained by the balance of hydrogenation and dehydrogenation at different given thermal energies, that is, at different temperatures. As annealing time increases to long hours, the effect of impurity dissolution may also degrade the lifetime τ_{other}, as in the case of the 900 °C anneals.

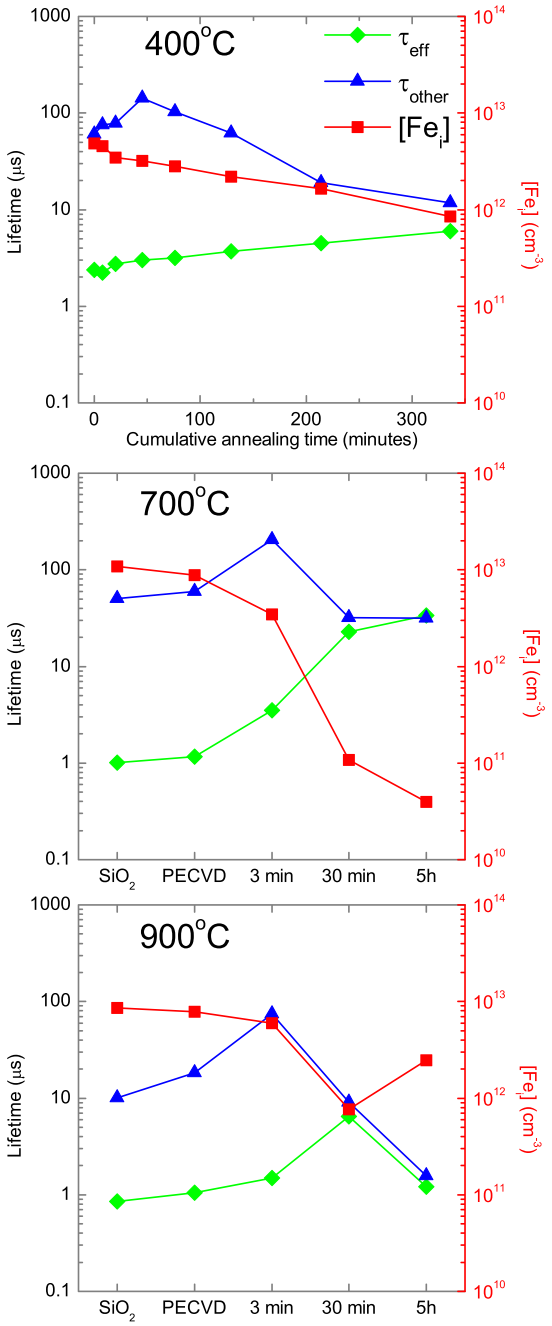

FIG. 9. Effective minority carrier lifetimes (τ_{eff}), lifetimes due to defects other than interstitial Fe (τ_{other}), and concentrations of interstitial Fe ([Fe_i]) of the same wafers before and after annealing for different times with SiN_x films present at 400 °C, 700 °C, and 900 °C. The lifetimes presented here are in the FeB paired state, at injection levels of $2 \times 10^{13} - 4 \times 10^{13}$ cm^{-3}. Lines are guides to the eyes.

IV. DISCUSSION

It was conjectured in Refs. 18 and 19 that the reduced recombination activity of metals during H ion bombardment at 300 °C (Ref. 19) and the decreased Fe_i concentrations during 400 °C hydrogen plasma exposure[18] resulted from hydrogen-enhanced metal diffusivity that drives more precipitation/gettering of dissolved metals. In this paper, we show that the Fe_i concentrations also decrease substantially after annealing at temperatures higher than the Fe solubility limit. This has also been reported previously[15–17] for other high temperature anneals, in which case the precipitation of Fe cannot explain the decreased [Fe_i]. In addition, the [Fe_i] images after annealing do not show the appearance or widening of the denuded zones near structural defects. Such denuded zones are characteristic of the inhomogeneous Fe precipitation process.[10]

We also considered the possibility that the substantial decline in [Fe_i] after annealing could be due to some uniform gettering sites by means of segregation at high temperatures, enhanced by the presence of hydrogen. For example, wafer

surfaces or uniformly distributed dense dislocations which cannot be spatially resolved by PL imaging. However, this was found to be unlikely. McLean *et al.*[17] reported that wafers which demonstrated an 80% decline in Fe_i concentrations after annealing with SiN_x films at 700–900 °C, temperatures at which the precipitation of Fe was not found in the preliminary test, recovered to the initial Fe_i concentrations and carrier lifetimes after annealing at 900 °C for 1 h in nitrogen with the SiN_x films removed, i.e., without the hydrogen source. McLean *et al.*[17] used FZ wafers with known concentrations of implanted Fe, and hence the impact of Fe precipitate dissolution on the $[Fe_i]$ is not present. If the aforementioned hypothesis were true, that is, the observed $[Fe_i]$ reductions were caused by the dissolved Fe_i atoms segregating to some uniform gettering sites within the mc-Si samples, the follow-up anneal at 900 °C for 1 h would result in further gettering of Fe_i, at a slower rate if assuming the process is enhanced by hydrogen, and the already gettered Fe should not be ejected back into the bulk resulting in a return of the $[Fe_i]$ to the pre-hydrogenated values. Therefore, the reductions in $[Fe_i]$ after high temperature anneals are not likely due to the gettering of Fe via segregation at high temperatures. Furthermore, these results show that in the absence of a hydrogen source, the process of dehydrogenation becomes dominant. This is a similar phenomenon to that observed by Rohatgi *et al.*[41] for the dehydrogenation of the previously hydrogenated EFG and string ribbon silicon, which demonstrates a significant drop in lifetime after firing the samples without the SiN_x films.

The significant reduction of Fe_i concentrations after annealing for a range of temperatures is therefore more likely related to the interaction of interstitial Fe and atomic hydrogen, the effect of which passivates the electrical activity of interstitial Fe in silicon. We propose that it may be the reaction of Fe and H atoms, resulting in less recombination active Fe-H complexes. The reaction is conjectured to be between positively charged Fe (Fe^+) and negatively charged H (H^-). However, other possibilities are not excluded. Although the fraction of negatively charged H (H^-) is small, the total H concentration from PECVD SiN_x is in the range of 10^{15}–$10^{16}\,cm^{-3}$,[20] and thus a small fraction of H^- is sufficient for the typical concentrations of dissolved Fe in mc-Si. The pairing of Fe^+ and H^- and the dissociation of Fe-H, that is, the process of hydrogenation and dehydrogenation, can explain the observed effectiveness of the $[Fe_i]$ reductions at various temperatures and times.

The activation energy for the hydrogenation of interstitial Fe was found to be in the range of 1.2 eV–2 eV in Ref. 17, and the binding energy of Fe and H was reported to be 1.5 eV in Ref. 11. The significant reductions of $[Fe_i]$ after annealing at 600–900 °C suggest that the forward reaction of hydrogenation is favoured over the reverse reaction of dehydrogenation.

V. CONCLUSION

In this study, we present experimental evidence for the hydrogenation of interstitial iron in multicrystalline silicon, upon annealing of PECVD SiN_x coated wafers for a range of temperatures from 400 °C to 900 °C and for times from minutes to hours. Decreases of more than 90% of the initial dissolved iron concentrations are observed after a 30-min anneal at 600–900 °C. At low temperatures where Fe precipitation also occurs, hydrogenation happens on a much faster time scale, acting as the dominant process. The most effective hydrogenation of dissolved Fe occurs at 700 °C, where 99% of the initial $[Fe_i]$ is hydrogenated after 30 min, and a longer annealing time drives even further reductions in $[Fe_i]$. This results in a large increase in the effective minority carrier lifetime for the Fe_i-limited mc-Si samples. Hydrogenation of other defects in the mc-Si, however, is more effective after shorter anneals. Further increases of the annealing time actually result in degrading τ_{other}, as dehydrogenation becomes dominant. Hydrogenation of Fe also occurs during the PECVD SiN_x deposition process, although the extent is less in comparison to annealing at higher temperatures. The results presented in this paper and those from high temperature hydrogenation studies[15–17] show that the reduced interstitial Fe concentrations after hydrogen incorporation are unlikely to be caused by an accelerated internal gettering of Fe at structural defects due to enhanced diffusivity of Fe in the presence of hydrogen. The hydrogenation process may be related to the pairing of positively charged Fe (Fe^+) with negatively charged H (H^-), forming less recombination active Fe-H complexes. For temperatures above 400 °C, simulations show that moderate excess carrier injection via illumination has little impact on the charge states of Fe and H, and this is experimentally confirmed by the similar observed hydrogenation processes of wafers annealed with and without illumination at 400 °C.

ACKNOWLEDGMENTS

This work was supported by the Australian Research Council and the Australian Renewable Energy Agency.

[1]A. A. Istratov, H. Hieslmair, and E. R. Weber, Appl. Phys. A **70**, 489–534 (2000).
[2]D. Macdonald, A. Cuevas, A. Kinomura, Y. Nakano, and L. J. Geerligs, J. Appl. Phys. **97**, 033523 (2005).
[3]T. Buonassisi, A. A. Istratov, M. D. Pickett, M. Heuer, J. P. Kalejs, G. Hahn, M. A. Marcus, B. Lai, Z. Cai, S. M. Heald, T. F. Ciszek, R. F. Clark, D. W. Cunningham, A. M. Gabor, R. Jonczyk, S. Narayanan, E. Sauar, and E. R. Weber, Prog. Photovoltaics: Res. Appl. **14**, 513–531 (2006).
[4]A. A. Istratov, H. Hieslmair, and E. R. Weber, Appl. Phys. A **69**, 13–44 (1999).
[5]S. P. Phang and D. Macdonald, J. Appl. Phys. **109**, 073521 (2011).
[6]P. Manshanden and L. J. Geerligs, Sol. Energy Mater. Sol. Cells **90**, 998–1012 (2006).
[7]M. Rinio, A. Yodyunyong, S. Keipert-Colberg, Y. P. B. Mouafi, D. Borchert, and A. Montesdeoca-Santana, Prog. Photovoltaics: Res. Appl. **19**, 165–169 (2011).
[8]M. D. Pickett and T. Buonassisi, Appl. Phys. Lett. **92**, 122103 (2008).
[9]S. M. Myers, M. Seibt, and W. Schröter, J. Appl. Phys. **88**, 3795–3819 (2000).
[10]A. Y. Liu and D. Macdonald, J. Appl. Phys. **115**, 114901 (2014).
[11]S. J. Pearton, J. W. Corbett, and T. S. Shi, Appl. Phys. A **43**, 153–195 (1987).
[12]C. Dubé and J. I. Hanoka, in *31st IEEE Photovoltaic Specialists Conference*, Lake Buena Vista, 2005 (IEEE, New York, 2005), pp. 883–888.
[13]M. Kouketsu and S. Isomae, J. Appl. Phys. **80**, 1485–1487 (1996).
[14]A. J. Tavendale and S. J. Pearton, J. Phys. C: Solid State Physi. **16**, 1665 (1983).

[15]L. J. Geerligs, A. Azzizi, D. H. Macdonald, and P. Manshanden, in *13th Workshop on Crystalline Silicon Solar Cell Materials and Processes*, Vail, Colorado, 2003 (National Renewable Energy Laboratory, Golden, Colorado, 2004), pp. 199–202.
[16]A. Azzizi, L. J. Geerligs, and D. Macdonald, in 19th European Photovoltaic Solar Energy Conference and Exhibition, Paris, 2004 (WIP Renewable Energies, Munich, 2004), pp. 1021–1024.
[17]K. McLean, C. Morrow, and D. Macdonald, in *4th World Conference on Photovoltaic Energy Conversion*, Waikoloa, 2006 (IEEE, New York, 2006), Vol. 1, pp. 1122–1125.
[18]P. Karzel, A. Frey, S. Fritz, and G. Hahn, J. Appl. Phys. **113**, 114903 (2013).
[19]R. Singh, S. J. Fonash, and A. Rohatgi, Appl. Phys. Lett. **49**, 800–802 (1986).
[20]M. Sheoran, D. S. Kim, A. Rohatgi, H. F. W. Dekkers, G. Beaucarne, M. Young, and S. Asher, Appl. Phys. Lett. **92**, 172107 (2008).
[21]B. J. Hallam, P. G. Hamer, S. R. Wenham, M. D. Abbott, A. Sugianto, A. M. Wenham, C. E. Chan, X. GuangQi, J. Kraiem, J. Degoulange, and R. Einhaus, IEEE J. Photovoltaics **4**, 88–95 (2014).
[22]T. Trupke, R. A. Bardos, M. C. Schubert, and W. Warta, Appl. Phys. Lett. **89**, 044107 (2006).
[23]H. C. Sio, S. P. Phang, T. Trupke, and D. Macdonald, Sol. Energy Mater. Sol. Cells **131**, 77–84 (2014).
[24]D. Macdonald, J. Tan, and T. Trupke, J. Appl. Phys. **103**, 073710 (2008).
[25]N. M. Johnson, D. K. Biegelsen, M. D. Moyer, V. R. Deline, and C. A. Evans, Appl. Phys. Lett. **38**, 995–997 (1981).
[26]G. Dingemans, W. Beyer, M. C. M. van de Sanden, and W. M. M. Kessels, Appl. Phys. Lett. **97**, 152106 (2010).
[27]M. Wilde, M. Matsumoto, K. Fukutani, Z. Liu, K. Ando, Y. Kawashima, and S. Fujieda, J. Appl. Phys. **92**, 4320–4329 (2002).
[28]R. A. Sinton and A. Cuevas, Appl. Phys. Lett. **69**, 2510–2512 (1996).
[29]G. Zoth and W. Bergholz, J. Appl. Phys. **67**, 6764–6771 (1990).
[30]D. H. Macdonald, L. J. Geerligs, and A. Azzizi, J. Appl. Phys. **95**, 1021–1028 (2004).
[31]A. Y. Liu, D. Walter, S. P. Phang, and D. Macdonald, IEEE J. Photovoltaics **2**, 479–484 (2012).
[32]D. Walter, A. Y. Liu, E. Franklin, D. Macdonald, B. Mitchell, and T. Trupke, in *38th IEEE Photovoltaic Specialists Conference (PVSC)* (2012), pp. 000307–000312.
[33]B. Herzog, G. Hahn, M. Hofmann, I. Romijn, and A. Weeber, in *23rd European Photovoltaic Solar Energy Conference*, Valencia, Spain, 2008 (WIP Renewable Energies, Munich, 2008), pp. 1863–1866.
[34]R. Krain, S. Herlufsen, and J. Schmidt, Appl. Phys. Lett. **93**, 152108 (2008).
[35]W. Shockley and W. T. Read, Phys. Rev. **87**, 835–842 (1952).
[36]R. N. Hall, Phys. Rev. **87**, 387 (1952).
[37]C. Herring, N. M. Johnson, and C. G. Van de Walle, Phys. Rev. B **64**, 125209 (2001).
[38]C. Sun, F. E. Rougieux, and D. Macdonald, "A unified approach to modelling the charge state of monatomic hydrogen and other defects in crystalline silicon," Phys. Rev. B (to be published).
[39]M. A. Green, J. Appl. Phys. **67**, 2944–2954 (1990).
[40]T. Buonassisi, A. A. Istratov, S. Peters, C. Ballif, J. Isenberg, S. Riepe, W. Warta, R. Schindler, G. Willeke, Z. Cai, B. Lai, and E. R. Weber, Appl. Phys. Lett. **87**, 121918 (2005).
[41]A. Rohatgi, D. S. Kim, K. Nakayashiki, V. Yelundur, and B. Rounsaville, Appl. Phys. Lett. **84**, 145–147 (2004).
[42]L. J. Geerligs, Y. Komatsu, I. Rover, K. Wambach, I. Yamaga, and T. Saitoh, J. Appl. Phys. **102**, 093702 (2007).
[43]J. Chen, T. Sekiguchi, D. Yang, F. Yin, K. Kido, and S. Tsurekawa, J. Appl. Phys. **96**, 5490–5495 (2004).